

CHAPTER 7

RESULTS

LITHIUM NICKEL MANAGANESE VANADATE BY THE POLYMER
PRECURSOR METHOD**7.1 Introduction**

As many attempts on the desirable high voltage behavior increasing since 1960's, reports on the development on the rechargeable lithium batteries has driven the urge to improve the structure for more stable and nanosized electrode. The supplementary of polymer source in the solution during synthesizing have proven the formation of nanostructured powder of the cathode. Moreover, the polymeric precursor is known to having a good dispersing agent throughout the polymer matrix [Subramania *et. al*, 2007]. It is also known for good gelling agents [Park *et. al*, 1997; Sun and Oh, 1997] where a homogeneous solution will be obtained and producing nanoparticle powder [Fey *et. al*, 2007].

The XRD experiment has been carried out to confirm the formation of the inverse spinel vanadate. The investigation in the weight relation upon temperature changes for the precursor was run by the TGA/DTGA technique. Consequently, chemical reaction will be proposed according to the weight loss/ gain curve. The images of the morphology of

the powder were analyzed by SEM and TEM instrumentations. The cyclic voltammetry, CV studies were employed for the electrochemical test.

7.2 Structural studies

7.2.1 X- ray diffraction (XRD)

$\text{LiNi}_{1-x}\text{Mn}_x\text{VO}_4$ – PP compound and its impurities were identified by powder XRD. The composition of $\text{LiNi}_{1-x}\text{Mn}_x\text{VO}_4$ by polymer precursor (PP) system is similar to that of the $\text{LiNi}_{1-x}\text{Mn}_x\text{VO}_4$ – SG system and presented in Table 7.1. The XRD spectra of polymer precursor derived $\text{LiNi}_{1-x}\text{Mn}_x\text{VO}_4$ ($0 \leq x \leq 1$) powder sintered at various temperatures presented in Figure 7.1 (V5), Figure 7.2 (V6), Figure 7.3 (V7), and Figure 7.4 (V8). Those spectrums were analysed and compared with the JCPDS data. For Figure 7.1, Figure 7.2 and Figure 7.3, the mixed phase of $\text{LiNi}_{1-x}\text{Mn}_x\text{VO}_4$ were identified for all sintering temperatures. The V8 composition which Ni was absent during the preparation, the peaks are only obtained for 500 °C and 600 °C due to the failure of sample collection where the sample cannot be collected after treated at higher temperature.

The XRD diffractogram for sample V5 and sample V6 are having mixed phases of $\text{LiNi}_{1-x}\text{Mn}_x\text{VO}_4$. The mixed phases gradually vanished as the peaks reduce upon Mn decrement. The system having the V7 composition reveals the formation of highly crystalline phase (the presence of [311], [220] and [111] peaks in the XRD diffractogram) follows the inverse spinel LiNiVO_4 structure upon annealing. This result again follows the literature [Lai *et. al*, 2002b] reported that the amount of Mn ratio fairly in the range of $0 \leq x \leq 0.4$ in the $\text{LiNi}_{1-x}\text{Mn}_x\text{VO}_4$ in which this system successfully prepared by applying 0.25 mole ratio of Mn. The calculated intensity ratio

of $I_{[220]}/I_{[311]}$ for inverse spinel $\text{LiNi}_{0.75}\text{Mn}_{0.25}\text{VO}_4$ by polymer precursor method is 0.42, 0.54, 0.34 and 0.58 for sample treated at 500 °C, 600 °C, 700 °C, 800 °C, respectively.

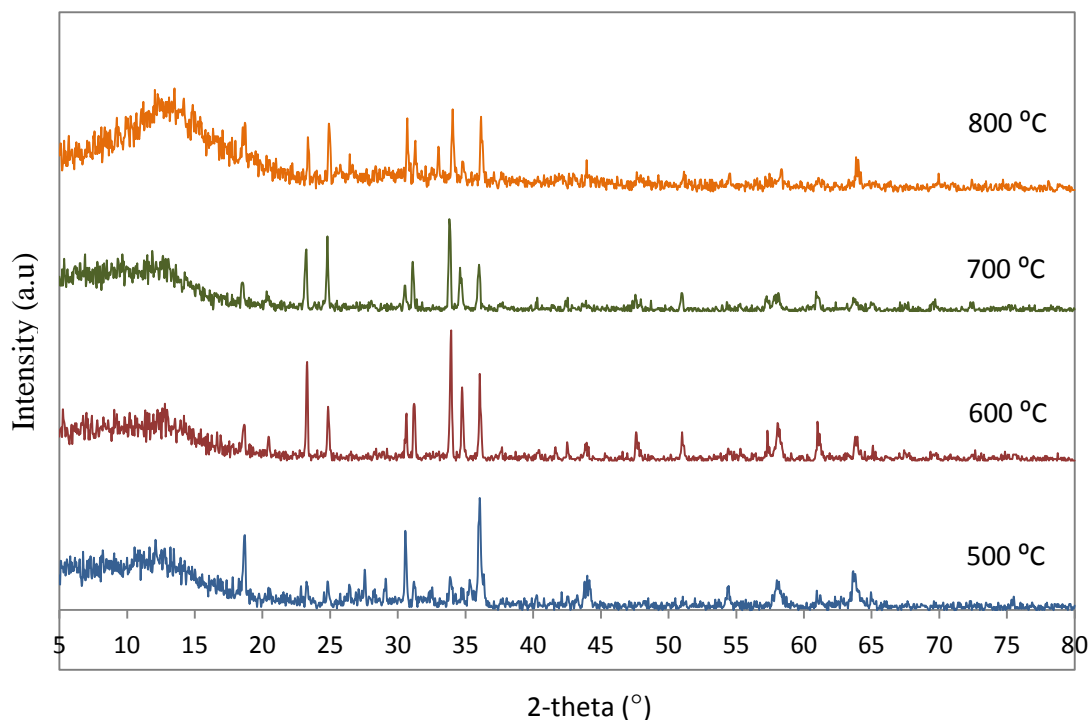


Figure 7.1: XRD pattern for V5 system

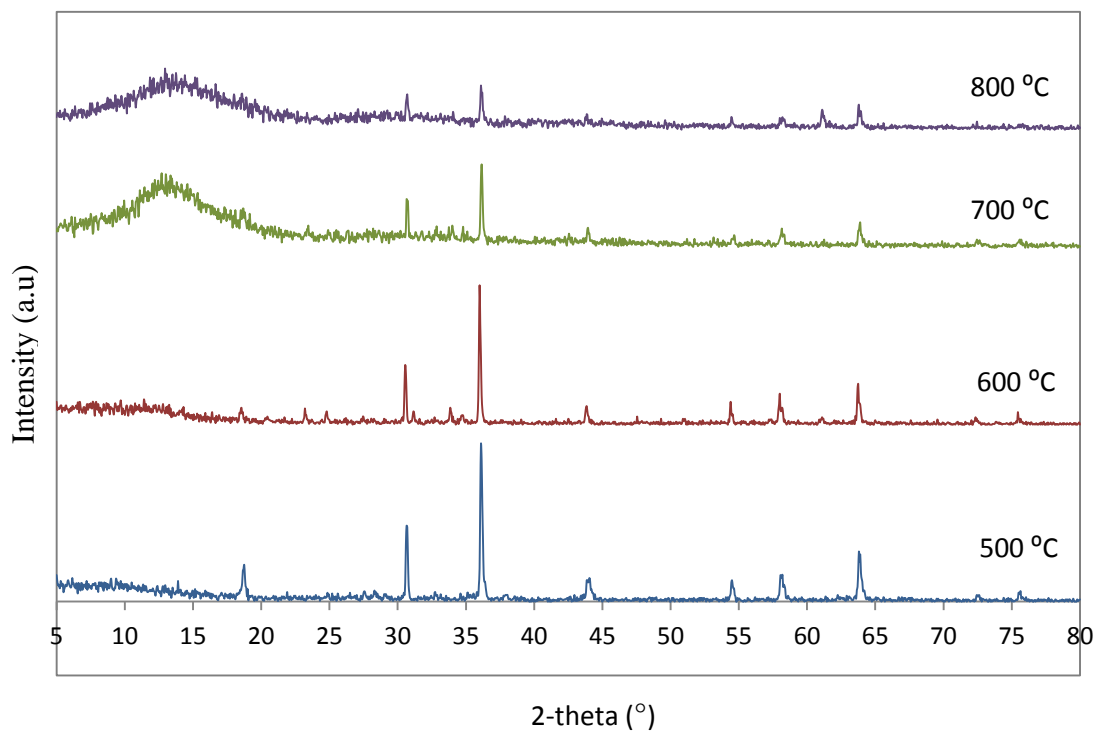


Figure 7.2: XRD pattern for V6 system

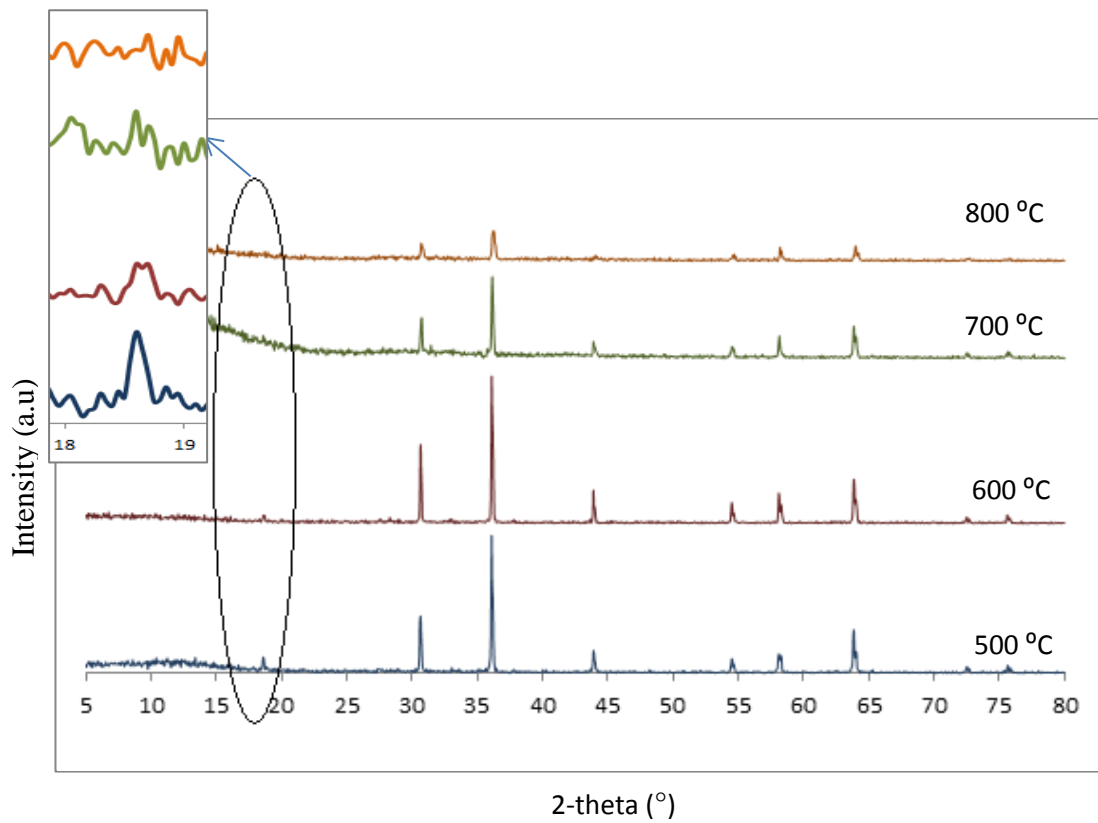
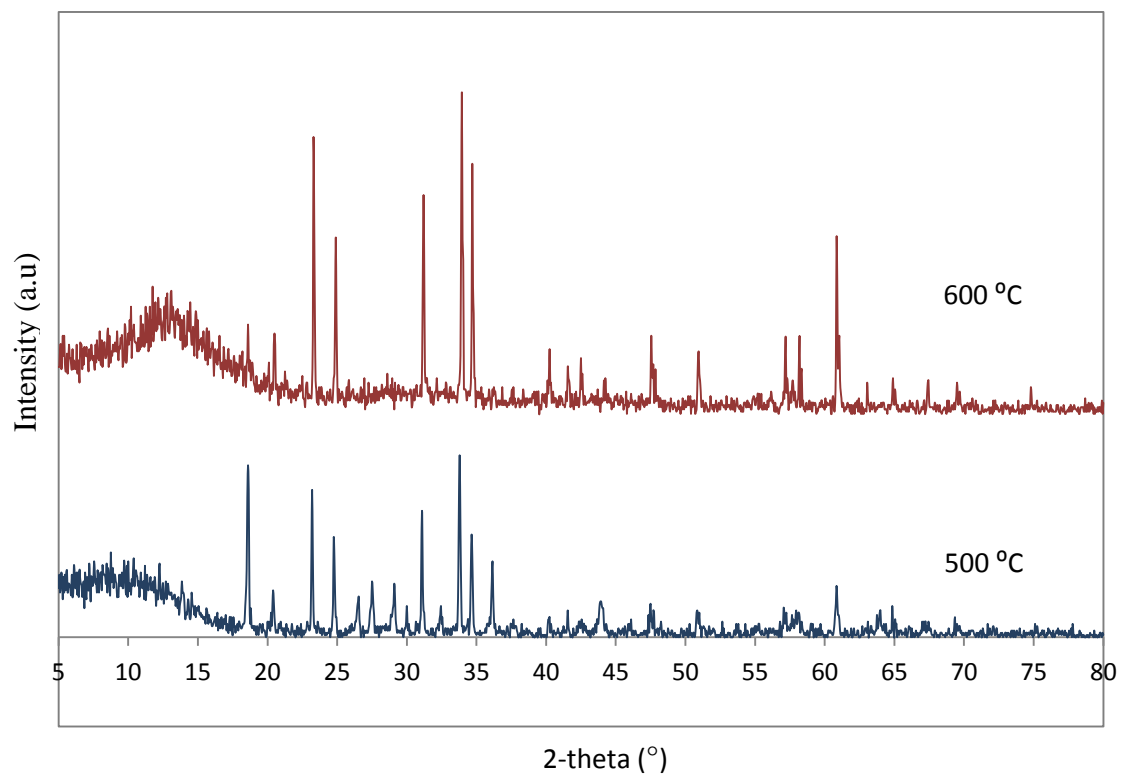
**Figure 7.3: XRD pattern for V7 system****Figure 7.4: XRD pattern for V8 system**

Table 7.1: Treatment conditions for preparation of $(\text{LiNi}_{1-x}\text{Mn}_x\text{VO}_4 - \text{PP})$ system

$\text{LiNi}_{1-x}\text{Mn}_x\text{VO}_4$	Ratio Ni:Mn
V5	0.25:0.75
V6	0.50:0.50
V7	0.75:0.25
V8	0.00:1.00

7.2.2 Crystallite size

The co-doped polymer system ($\text{LiNi}_{1-x}\text{Mn}_x\text{VO}_4 - \text{PP}$) was determined by using the Scherrer formula in order to evaluate the behaviour of the crystal sizes. Yet again, the value was obtained by using the powder XRD data given in the analysis. The [3 1 1] plane peak of the system was chosen for using the Scherrer formula to obtain the crystallite size observed in the XRD pattern. The calculated crystallite size is shown in Table 7.2. It should be bear in mind that the crystallite size obtained by Scherrer equation provides the information on the estimated average size of the crystal powder. The crystallite size for the powder exhibit 39.53 nm for the polymer precursor mixed doped system at both 500 °C and 600 °C. At higher sintering temperature, the crystalline powder forms smaller crystal size of 35.47 nm and 19.82 nm at 700 °C and 800 °C, respectively.

Table 7.2: Crystallite size values for the $\text{LiNi}_{0.75}\text{Mn}_{0.25}\text{VO}_4$ -PP) system

Temperature (°C)	Crystallite Size (nm)
500	39.53
600	39.53
700	35.47
800	19.82

7.2.3 Lattice constants and the volumes of crystal cell

For cubic crystal structure, the lattice parameter, a can be calculated by the powder XRD data available in the analysis. The lattice constant can be obtained by using the Bragg's formula. The data was chosen at the most intense [311] peak. The lattice constants with respective compound of each system based on the obtained 2- theta value of the [h k l] values are tabulated in Table 7.3.

Table 7.3: Lattice constant value for doped $\text{LiNi}_{1-x}\text{Mn}_x\text{VO}_4$ -PP ($0 \leq x \leq 1$) system

System	2θ (°)	θ (°)	d obs.	a (Å)
$\text{LiNi}_{1.00}\text{Mn}_{0.00}\text{VO}_4$	36.238	18.119	2.476	8.215
$\text{LiNi}_{0.25}\text{Mn}_{0.75}\text{VO}_4$	36.054	18.027	2.489	8.255
$\text{LiNi}_{0.5}\text{Mn}_{0.5}\text{VO}_4$	36.121	18.061	2.484	8.238
$\text{LiNi}_{0.75}\text{Mn}_{0.25}\text{VO}_4$	36.133	18.067	2.483	8.235

The calculated lattice constant are presented by plotting the variation of the lattice constant, a values and cell volume, V with the manganese content, x for the mixed-doped system. The manganese, Mn substitution has influence the a and the cell volume of the doped vanadates. The Ni is having 0.69 Å ionic size [Rubi *et. al*, 2007] while the Mn^{2+} is having 0.83 Å [Shannon, 1976].

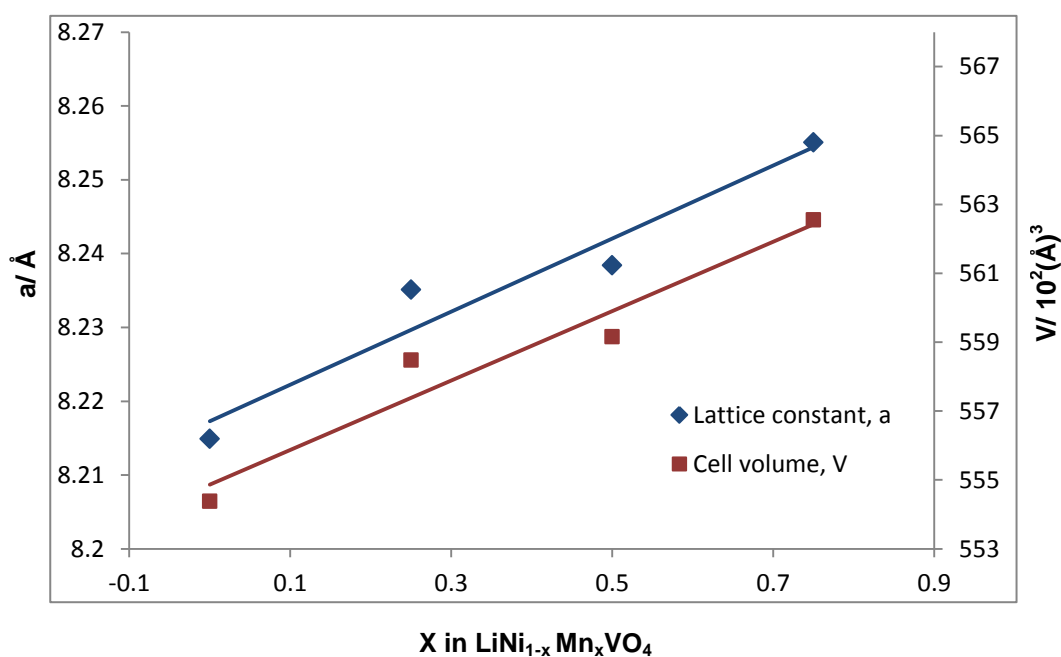
**Figure 7.5: Lattice constant, a and cell volume, V for $\text{LiNi}_{1-x}\text{Mn}_x\text{VO}_4$ – PP ($0 \leq x \leq 1$) system at 600 °C**

Figure 7.5 represents the lattice constant, a and the cell volume, V for the $\text{LiNi}_{1-x}\text{Mn}_x\text{VO}_4 - \text{PP}$ system. The results show that the lattice parameter increases with increasing of Mn content. These plots also follow the trend for result obtained by Lai and his research group reported in 2002 [Lai *et. al*, 2002b] as presented in Figure 7.6. The increase of the lattice parameter may correspond to the ionic radii of the Mn^{2+} ions. In this case, the increase of lattice parameters is due to the substitution of larger Mn^{2+} ion by increasing value of Mn in the system.

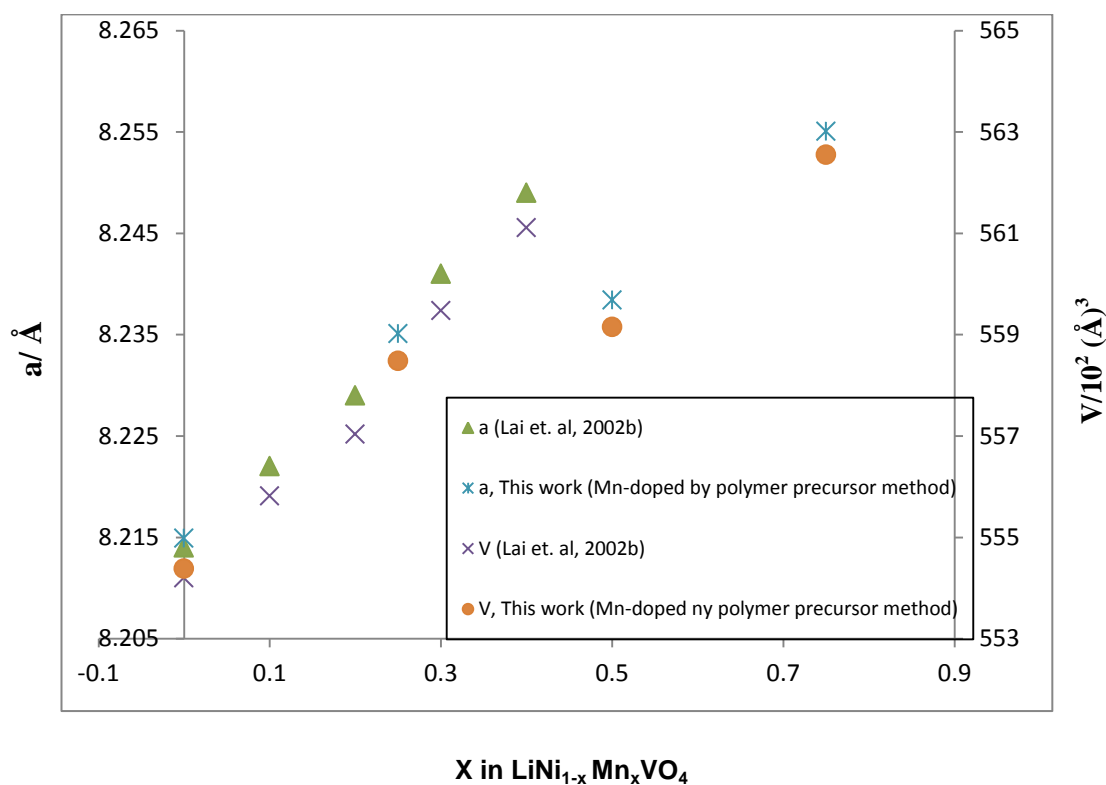


Figure 7.6 Lattice constants and the volumes of crystal cell for $\text{LiNi}_{1-x}\text{Mn}_x\text{VO}_4 - \text{PP}$ ($0 \leq x \leq 1$) at 600 °C.

For Lai *et. al*, (2002b) temperature is 750 °C.

7.3 Chemical Reaction

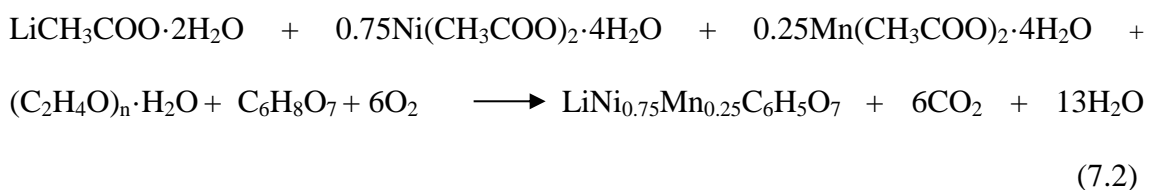
The formation process for the $\text{LiNi}_{1-x}\text{Mn}_x\text{VO}_4$ - PP was analysed based on the observation upon solution mixing and the possible reaction that happen during the synthesis. The reaction mechanisms are also discussed to study the chemical behaviour for the prepared compound.

A clear dark purple solution was observed after addition of the acid into the solution. The reaction of the citric acid with the NH_4VO_3 will produce V_2O_5 . The corresponding reaction can be described as:

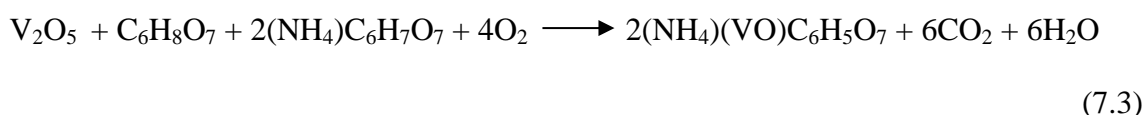


A gas evolution was observed after the mixing process took place in the solution where the acetate reactants react with the citric acid. This reaction happen when the metal acetates was mixed with the citric acid, $\text{C}_6\text{H}_8\text{O}_7$ forming a complex metal citrates in the process. Therefore, the CO_2 gas and $\text{LiNi}_{1-x}\text{Mn}_x\text{C}_6\text{H}_5\text{O}_7$ were produced:

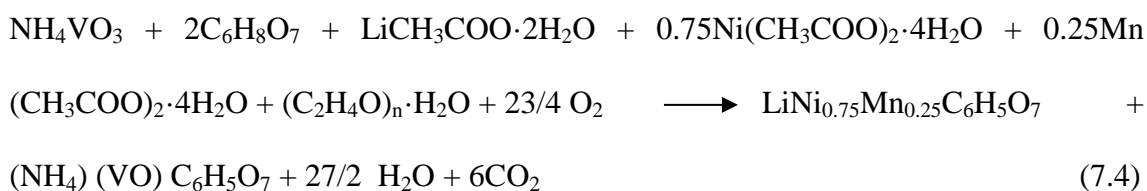
After prolonged heating condition, the byproduct obtained may result as follows:



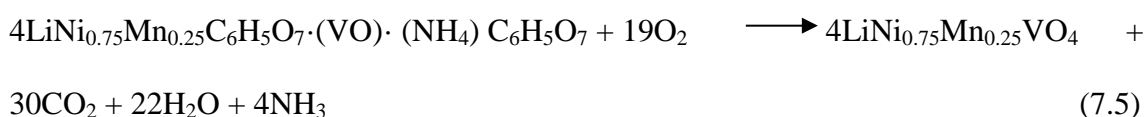
The V_2O_5 behaves as oxidant in the acidic solution according to Tsaramyrsi et al. (2001). Thus, the reaction of the citric acid with the oxidant, the solution will form an acid complex. The oxidation state can be reduced to V(IV) from V(V) in V_2O_5 with the gas evolution, forming the $(\text{VO})^{2+}$ ion. Subsequently, the reaction between the $(\text{VO})^{2+}$ ion with $(\text{NH}_4)\text{C}_6\text{H}_7\text{O}_7$ will produce $(\text{NH}_4)(\text{VO})\text{C}_6\text{H}_5\text{O}_7$.



The total reaction of those corresponding chemical reaction can be written as:



Below is the proposed total decomposition equation in air atmosphere that can be written as:



7.4 Thermogravimetric Analysis (TGA)

The resulting compound from the dried gel of the polymer precursor $\text{LiNi}_{1-x}\text{Mn}_x\text{VO}_4$ was collected after the product turns into powder form. The TGA analysis was carried out using the precursor obtained by the synthesized method at temperature range of

room temperature up to 750 °C. Figure 7.7 represents the TGA and DTGA plots of the mixed doped vanadate by polymer precursor method.

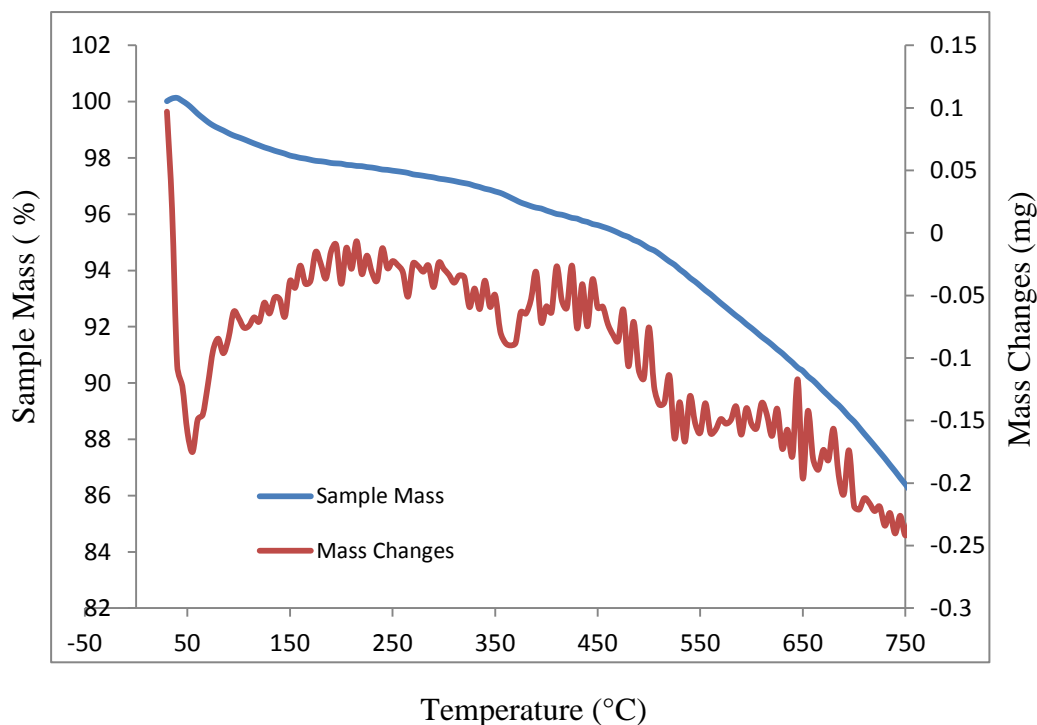


Figure 7.7: TGA and DTGA curve of the $\text{LiNi}_{1-x}\text{Mn}_x\text{VO}_4$ - PP precursor

As expected, the prominent endothermic peak weight loss of about 2.3 % was observed due to the evaporation of water from the powder and lithium acetate decomposition. Subsequently, the second endothermic peak located at 355 °C. This phenomenon can be attributed by decomposing process by the manganese acetate that present in the compound. There is no obvious weight loss behaviour as the TGA curve was smoothly plotted although small exothermic peaks present in the DTGA curve. Those small and close peaks are observed almost showing the refined curved peaks compared with the sol- gel mixed doped system. This means that the decomposition of the intermediates or the complexes do undergoes small weight loss. This result indicates that the compound are forming stable phase through continuous reacting temperature. The decomposition

process in the system hold a total weight loss of about 14.37 % based on the TGA analysis.

7.5 Morphology studies

7.5.1 Scanning Electron Microscopy (SEM)

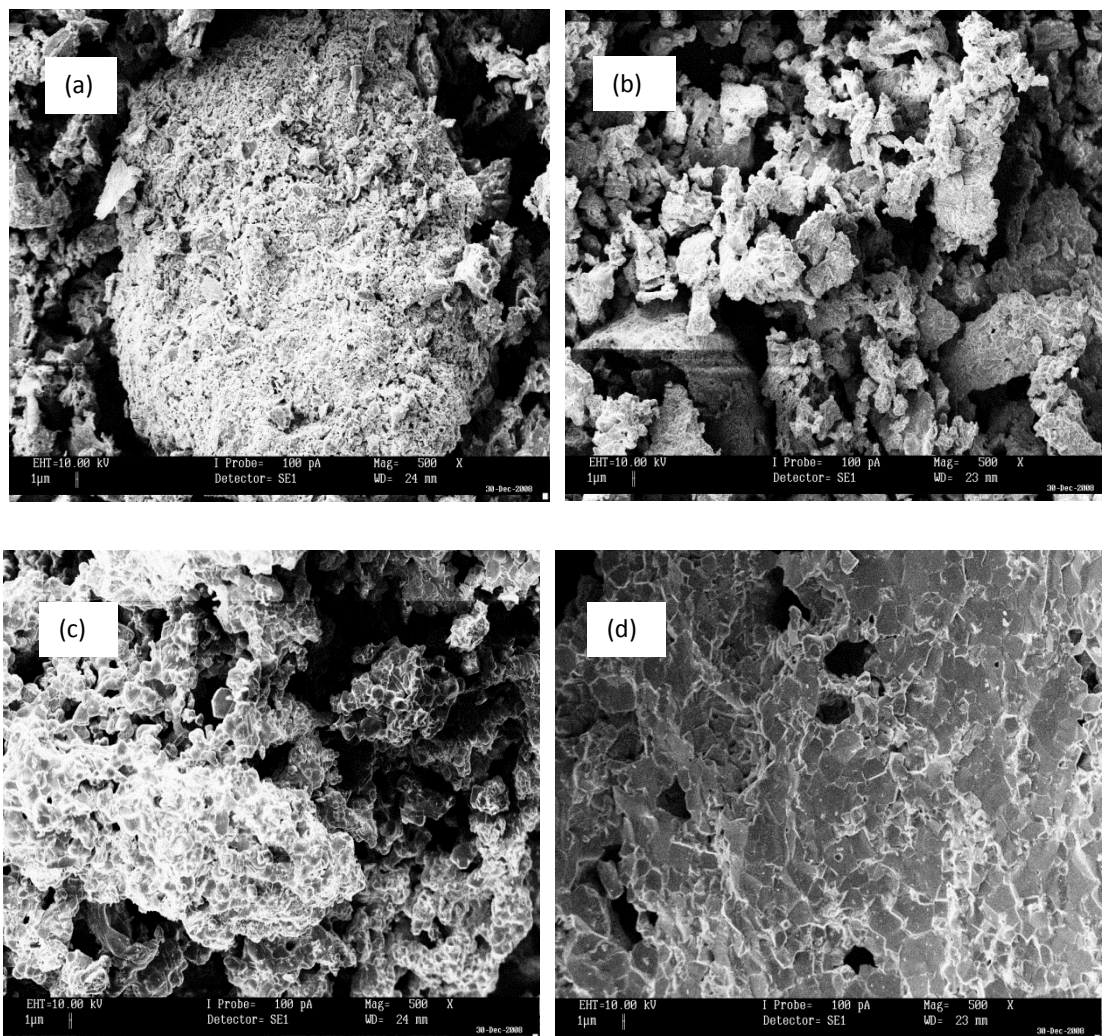


Figure 7.8: Surface morphology of $\text{LiNi}_{0.75}\text{Mn}_{0.25}\text{VO}_4 - \text{PP}$ system at (a) 500 °C; (b) 600 °C; (c) 700 °C; (d) 800 °C with 500X magnification

The SEM images for the mixed doped inverse spinel $\text{LiNi}_{0.75}\text{Mn}_{0.25}\text{VO}_4 - \text{PP}$ are shown in Figure 7.8 to investigate the effect of the surface morphology of adding doping

material, Mn and polymer (PEG) at different sintering temperatures. The mixing of dopant and the polymer source did not change much on the particle morphology as they exhibit brittle-like powder as shown in Figure 7.8 (a and b). This behaviour demonstrates the same phenomenon in three systems discussed previously that happens at lower sintering temperature.

The particle of the powder grew larger producing spherical and smooth particle edges as the temperature increases as displayed in Figure 7.8 (c). The surface in Figure 7.8 (d) portrays flat and densified morphology with much less voids as the precursor of the system achieved at 800 °C. Besides, the microstructure possesses uniform and cubic octahedral crystal in the matrix region.

However, as we already discussed the effect of synthesizing method on temperature variations, this work have also consider the issue of the particle formation upon temperature. Figure 7.9 depicts the effect of available systems in this work upon the same sintering heating treatment.

It is well understood that the particle specimens exhibit growing spherical particle as the temperature raised to higher value as mentioned in all systems in this work. On the other hand, the observed particle cluster has developed upon different systems as shown in Figure 7.9 (a to c) the same calcination temperature. Nevertheless, the shrinkage particle was obtained for $\text{LiNi}_{0.75}\text{Mn}_{0.25}\text{VO}_4 - \text{PP}$ system upon addition of polymer source as shown in Figure 7.9 (d).

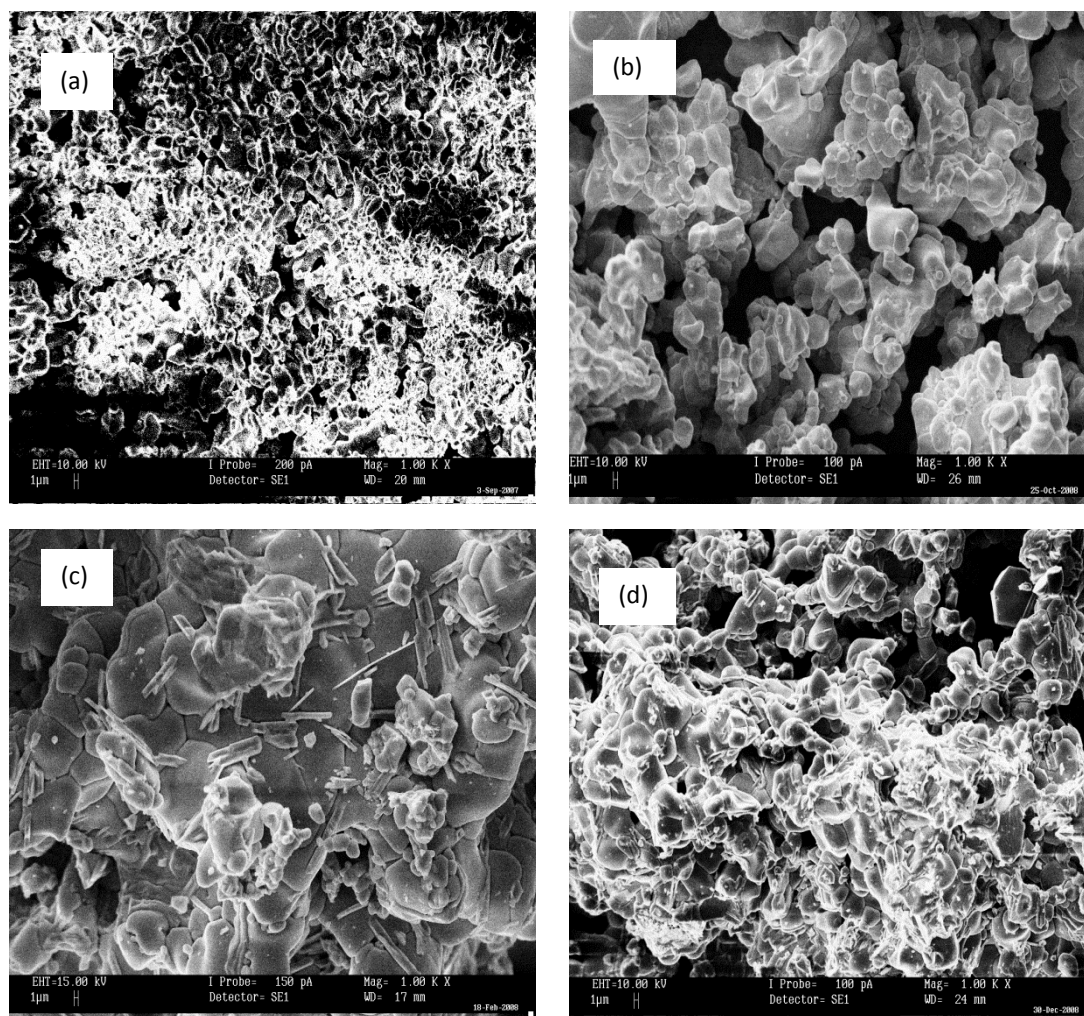


Figure 7.9: Surface morphology of (a) LiNiVO_4 - SG system; (b) LiNiVO_4 - PP system; (c) $\text{LiNi}_{0.75}\text{Mn}_{0.25}\text{VO}_4$ – SG system; (d) $\text{LiNi}_{0.75}\text{Mn}_{0.25}\text{VO}_4$ – PP system at 700 °C with 1.00 kX magnification

This manner was highly believed that the polymer source not only behaves as complexing agent between metal cation and carboxylic acid for better dispersity, it is also promotes homogeneity distribution on the positive ions through polymeric network forming nanosized particles [Song and Lee, 2002; Vivekanandhan *et. al*, 2004; Vivekanandhan *et. al*, 2005; Fey *et. al*, 2006a; Fey *et. al*, 2006b; Fey *et. al*, 2007].

7.5.2 Transmission Electron Microscope (TEM)

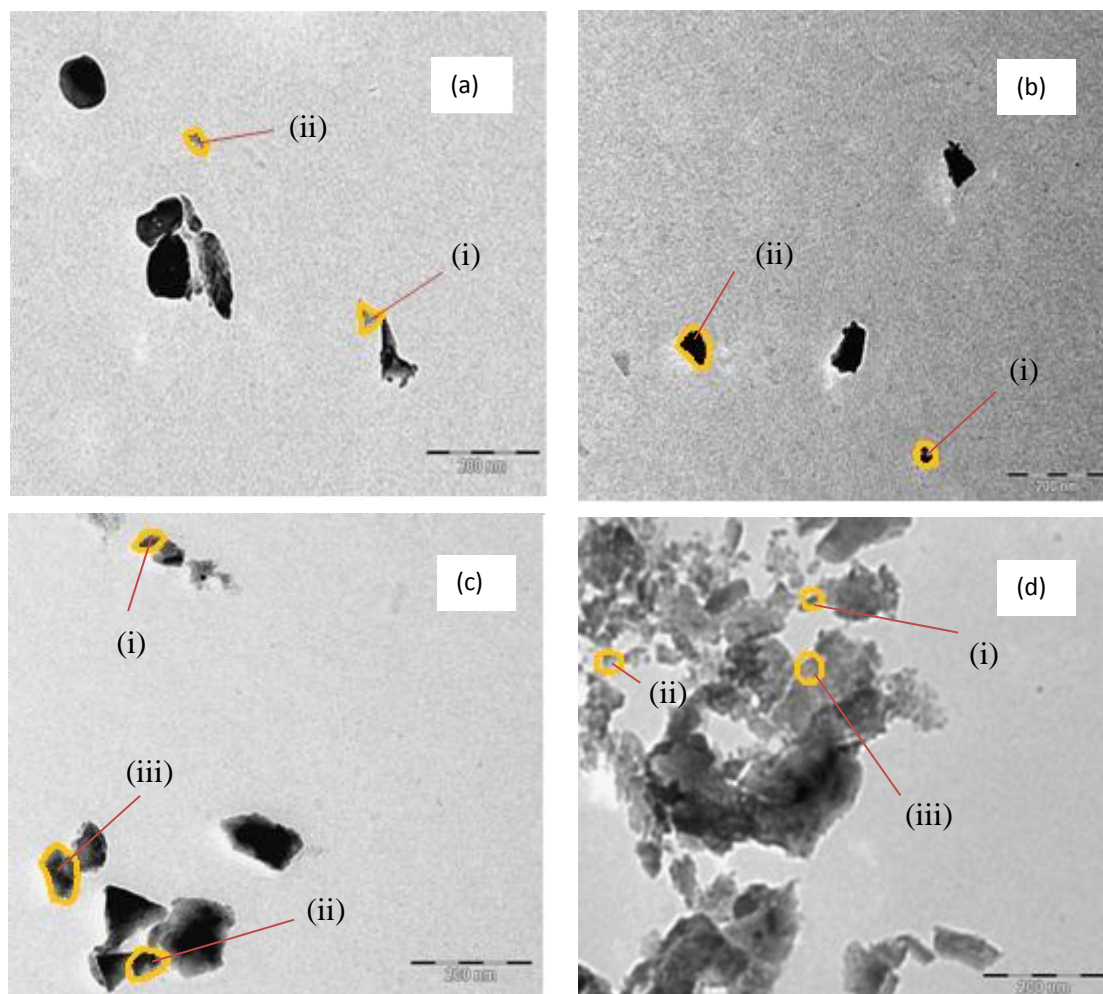


Figure 7.10: TEM images of $\text{LiNi}_{0.75}\text{Mn}_{0.25}\text{VO}_4$ – PP system at (a) 500 °C; (b) 600 °C; (c) 700 °C; (d) 800 °C

The TEM images were performed to investigate the actual particle size range for the prepared compound by polymer precursor method. The depicted image of synthesized compound shown in Figure 7.10 (a) was found to have single spherical nanoparticles away from each other. The particle size labeled in Figure 7.10 a (i) and Figure 7.10 a (ii) are 46.7 nm and 40.0 nm respectively. The sample sintered at higher temperature shown in Figure 7.10 (b and c) revealed the single sharp edge particle in the compound with almost similar shapes. Figure 7.10 b (i) is 46.1 nm while the particle size in Figure 7.10 b (ii) is 61.5 nm. The particle size in Figure 7.10 c (i), Figure 7.10 c (ii) and Figure 7.10

c (iii) are 37.5 nm, 62.5 nm and 75 nm, respectively. As the temperature rose up to the highest (800 °C), the structure of $\text{LiNi}_{0.75}\text{Mn}_{0.25}\text{VO}_4 - \text{PP}$ system become well dispersed having narrow distribution with smaller particle size as presented in Figure 7.10 d (i), Figure 7.10 d (ii) and Figure 7.10 d (iii) at 18.75 nm, 25 nm and 37.5 nm, respectively.

7.6 Cyclic voltammetry (CV)

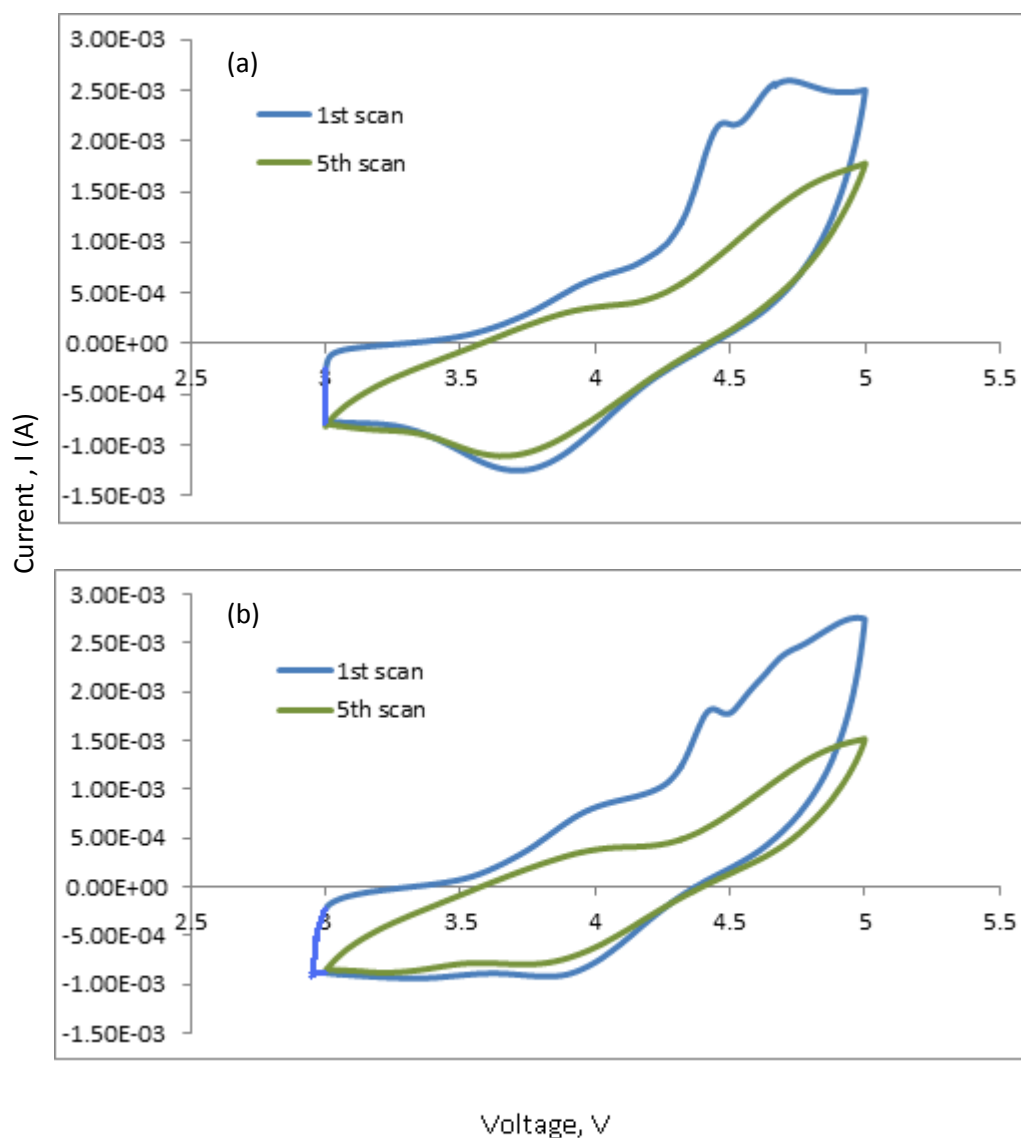


Figure 7.11: Cyclic voltammograms for Li/ $\text{LiNi}_{0.75}\text{Mn}_{0.25}\text{VO}_4 - \text{PP}$ electrode system in 1 mol dm^{-1} LiPF_6 in 1:2 by (vol/ vol%) EC/DMC at scan rate of 1 mV/s (a) cathode sintered at $600 \text{ }^\circ\text{C}$; (b) cathode sintered at $800 \text{ }^\circ\text{C}$

The cyclic voltammetry for the $\text{LiNi}_{0.75}\text{Mn}_{0.25}\text{VO}_4 - \text{PP}$ versus Lithium is shown in Figure 7.11. The cell using the compound as the cathode material was measured for the first five scan and in room temperature. The obtained peaks recorded suggest the reversible behavior of the material in the system. The voltammogram of the doped $\text{LiNi}_{0.75}\text{Mn}_{0.25}\text{VO}_4$ by polymer precursor method demonstrates the identical behavior with the doped system by sol-gel method. There is an anodic peak at 4.4 V as shown in Figure 7.11 (a). The cathodic peak was observed at 3.7 V. As the cycling number increases, the area of the curve was reduced with disappearance of the obvious 4.4 V and on the forward scan.

The cyclic voltammogram plots for the same compound at higher calcination temperature in Figure 7.11 (b) show anodic peak at 4.4 V. The cathodic scan shows intercalation of Li^+ at 3.7 V at the 1st scan. There was no obvious shift of the reduction potential upon increasing number of cycle. However, the area under curve decreases upon few cycles suggesting the decay in capacity in the cell system.

7.7 Summary

In this work, the dopant material using the manganese acetate has successfully synthesized via polymer precursor method and assisted by the citric acid for the $\text{LiNi}_{0.75}\text{Mn}_{0.25}\text{VO}_4$ system. The TGA test for the obtained precursor was held in the thermal chamber for the thermal studies and the chemical reaction can be proposed in relation of the thermal analysis. The total weight loss displays the weight loss of 14.37 % in this work.

The obtained particle size behaviour was identical to that of the mixed doped via the sol gel method. Similarly, the crystal size of the system decrease with increasing the firing temperature. The crystal sizes were ranging from the 39.53 nm down to 19.82 nm upon increasing temperature. The morphology studies demonstrate the corresponding result obtained from the TEM images.

The voltammogram from the cyclic voltammetry test show obvious oxidation/ reduction peak in the cell system. Similarly to the mixed doped via sol gel system, the noticeable peak is only presence at the 1st scan of the redox system. The size of the curve area initially slightly bigger and subsequently decreases upon further scans.